Line profiles of the P_α and P_β transitions in He II and broadening of C IV lines at high electron densities

U. Ackermann,* K. H. Finken,† and J. Musielok‡
Institut für Experimentalphysik V, Ruhr-Universität Bochum, D-4630 Bochum, Federal Republic of Germany
(Received 13 December 1983; revised manuscript received 12 September 1984)

Line shapes of P_α ($\lambda=4686$ Å) and P_β ($\lambda=3203$ Å) of He II and of some C IV lines are analyzed for plasmas in the parameter range $10^{23}\ \mathrm{m}^{-3} \le N_e \le 5\times10^{23}\ \mathrm{m}^{-3}$ and $kT_e \le 11$ eV for the electron density and temperature. The light source is a gas-liner pinch, a quite new device, which is optimized to produce a homogeneous test plasma. The light emission of helium and carbon takes place only from a very limited region of the central plasma. The spectral lines are analyzed with respect to the line broadening and the He II lines additionally to the asymmetry. For the investigation of the C IV lines, transitions were selected which came from different upper energy levels and which were broad and intense enough for a reliable measurement. They cover the wavelength region 948 to 5805 Å. By comparing the results with different theories, it is found that the experimental values are about a factor of 2 higher than the theoretical ones.

I. INTRODUCTION

The broadening of spectral lines of hydrogenic ions yields a reliable method to determine the electron density in plasmas. At lower temperatures and densities light ions are used while at high densities and temperatures as, e.g., in the laser fusion application, heavy ions are adequate. The line broadening of nonhydrogenlike lines is more complex because more electronic states are involved. Though these lines are also used for determining the electron density of "laser fusion" pellets from the line broadening there is still a gap between detailed measurements and recent calculations. Up to now there have been only few experiments to test the accuracy of these calculations.

The aim of this paper is to present data for hydrogenlike lines and for lithiumlike lines; more precisely, for He II and C IV lines. The gross properties of the shape of the He II lines are pretty well understood, though there are still discrepancies about the broadening for a given electron density. More controversial is the question of how strongly details of the line shape are influenced by higher-order perturbation effects. A line shift can be caused by different mechanisms: by the polarization of the plasma,[1] by close[2,3] and by distant electronic collisions.[4] The shift can be to shorter or larger wavelengths, depending on the specific line. Additionally, the lines show an asymmetry, which resembles to a certain degree the line shift. The main reason for an asymmetry of the lines is the quadrupole effect. Though the principles of some mechanisms leading to line shifts or asymmetries are understood, it is not at all known how important the individual process is.

Recently measurements were made by Pittman and Fleurier[5] concerning the shift of P_α (4686 Å) of He II. The electron density varied from 2×10^{22} to $2\times10^{23}\ \mathrm{m}^{-3}$, and the temperature was about $kT_e=4$ eV. In agreement with the plasma polarization model a red shift proportional to the electron density was observed. The effect of ionic quadrupole fields was taken into account but proved to amount to only 30% of the shift at the given conditions. Distant electronic collisions were neglected. It is expected that the polarization shift depends inversely on the electron temperature. Our experiment yields a homogeneous plasma so that error bars of the measured data are smaller than 10%. One of the main concerns of this paper will be to compare the line shape with the theory and with the experiment of Pittman and Fleurier.[5]

Lithiumlike ions resemble the hydrogenlike ones as they have only one electron in the outer shell. The higher atomic states become more and more hydrogenlike, i.e., nearly degenerate. The lower states, on the other hand, are isolated so that the lines from the lithiumlike ions represent a transition from well-separated lines to degenerate lines. The lithiumlike-ion lines, however, are not nearly so well understood and well investigated as the hydrogenlike ones. Therefore, we do not investigate the details of the lines here but only the broadening.

In Sec. II at first the experiment is described followed by a determination of the main plasma parameters (electron density and temperature) and the distribution of the test gas inside the pinch column. Because the He II lines are also used for evaluating the electron density we continue with the discussion of further properties of these lines: the widths and asymmetries of these lines. After a discussion of the observations the theory of isolated lines is briefly repeated and results of the broadening of 12 C IV lines are reported.

II. EXPERIMENT

The plasma source is a gas-liner pinch; important features of the device are published elsewhere[6–8] so only the principle of the device as shown in Fig. 1 is briefly reviewed. The gas-liner pinch is topologically a z pinch. Its special properties are derived from the gas inlet system: two fast valves inject gas streams into the discharge chamber, one jet along the axis (test gas) and one gas shell concentric to the latter one (driver gas). The driver plasma absorbs the energy like a gaseous liner from the outer circuit and is accelerated by the magnetic piston towards the center. There it hits the central test gas and heats it. To achieve a homogeneous test plasma as desired for plas-

 ©1985 The American Physical Society

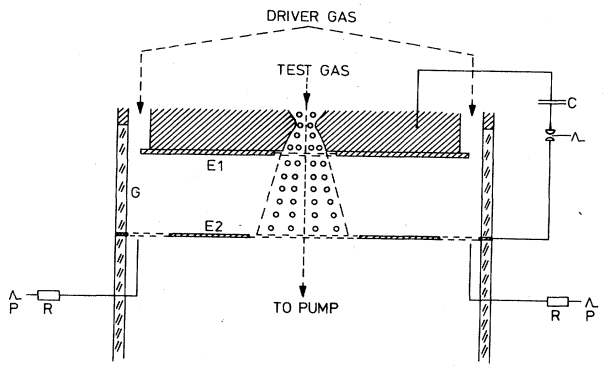

FIG. 1. Schematic drawing of the gas-liner pinch. The storage capacitor C contains an energy of 1.2 kJ at a voltage of 20 kV. $E1$ and $E2$ are the electrodes, G is a glass wall and P a preionization circuit.

ma spectroscopy, the test gas has to be confined to the central part of the device. This is achieved by selecting the separation between the electrodes small compared to the radius of the driver gas shell. For the present investigations, the interelectrode distance amounts to 5 cm and the driver gas shell radius to 8 cm. The other important data of the device are: stored electrical energy, 1.2 kJ; ringing time, 2.5 μs; driver gas pressure ~ 0.25 Torr H_2; amount of test gas $\sim 1-10\,\%$ of the driver gas.

The pinch resembles a dynamic z pinch, with the pinch phase determined by the inertial forces of the converging plasma and not by the magnetic field pressure. This condition gives about 10^{24} particles per m^3 during the dense plasma phase. Because of the lack of pressure equilibrium the plasma column lives only for a sound transit time, i.e., for 300 ns or slightly longer at the given conditions. It is known, however, that these dynamically confined plasmas are very reproducible and show steep density gradients at the boundary while they are flat at the center.

The continuum light of the plasma is recorded via a photomultiplier and an oscilloscope; as the continuum light emissivity is proportional to the square of the electron density, this signal is used as monitor signal clearly indicating the time of maximum compression. To obtain the absolute value of the continuum light another calibrated spectrometer was added for some measurements. For analyzing spectral lines, the plasma light is focused side-on to the entrance slit of a 1-m monochromator. In the exit slit plane, an OMA II array (detector 1420, EG&G) records the interesting part of the spectrum. The optical multichannel analyzer (OMA) system is pulsed for 20 ns for strong spectral lines and for 50 ns for weaker lines. Tests confirmed that this time resolution is sufficient.

For calibration, all OMA channels have to be exposed to the same light density. This was done in a nonpulsed mode by placing neutral-density filters in front of the detector and by exposing it to room light, or in the pulsed mode by opening the entrance slit of the monochromator and by looking at the continuum light of the discharge. It was found that the homogeneity of the channels is better than 5%. For C IV lines in the vacuum-ultraviolet (vuv) spectral range a 1-m normal incidence spectrometer is used for wavelengths $\lambda < 1500$ Å. The resolution amounts to 0.17 Å which is at least a factor of 2 smaller than the narrowest lines analyzed by us. The results discussed later have, of course, been corrected for the instrumental broadening.

III. DETERMINATION OF THE PLASMA PARAMETERS

The most important parameter for the line broadening is the electron density. This quantity is derived here in two different ways: from the broadening of P_α of He II and from the absolutely measured continuum radiation.

The technically simplest method is the evaluation of N_e from the half-width of P_α. It is simple insofar as no Abel inversion is required for the gas-liner pinch. It will be shown below that the emission of P_α occurs from a volume of constant electron density, i.e., the half-width does not change with the radius of the pinch column. Several theories have been performed to relate the width of P_α to the electron density. The best empirical relation as proposed by Pittman and Fleurier[5] is

$$N_e = 2.04(\Delta\lambda_{\mathrm{FWHM}}^{1.21})10^{22}\ \mathrm{m}^{-3}\ , \tag{1}$$

where $\Delta\lambda_{\mathrm{FWHM}}$ is the full half-width of P_α in angstroms. Theoretically the broadening depends also on the electron temperature. For electron densities of the order of 10^{24} m^{-3} this dependence is very weak; different calculations[1,9] predict a temperature variation of $\Delta\lambda_{\mathrm{FWHM}}$ for $2 \leq kT_e \leq 16$ eV of less than 5%. This small effect is neglected.

Figure 2(b) shows the time dependence of the electron density in the central part of the plasma derived using this equation. The time scale there and in following discussions is normalized to the continuum light signal which is shown in Fig. 2(c) for comparison. The central electron density reaches a maximum value of 5.6×10^{23} m^{-3}; this value is nearly constant for about 70—100 ns. Then, the density drops with a time constant of about 200 ns. The density rises earlier than the continuum light emission, reaching the maximum value 50 ns before the maximum of the monitor signal. This early rise is consistent with the assumption that the core density of the column is constant but that the diameter increases because more particles are swept inwards. Coincident with the increase of the continuum light a strong increase of the light emission at P_α is observed which is explained by the ionization time of He I.

The determination of N_e by the absolute measurement of continuum radiation is performed to check both the validity of (1) and to obtain the radial distribution of the electron density as compared to the volume from where the test gas is emitted. To avoid statistical variations of the discharge, the whole continuum emission is recorded during one discharge. For this purpose the entrance slit of the spectrometer is imaged across the pinch column and the OMA is rotated so that light of the one wavelength but at different radial positions is detected. The measurement is made absolute by adding a separate spectrometer-multiplier system, which is absolutely calibrated by a tungsten ribbon lamp. An Abel inversion is performed after smoothing out the photon noise. The electron density is calculated from the continuum emis-

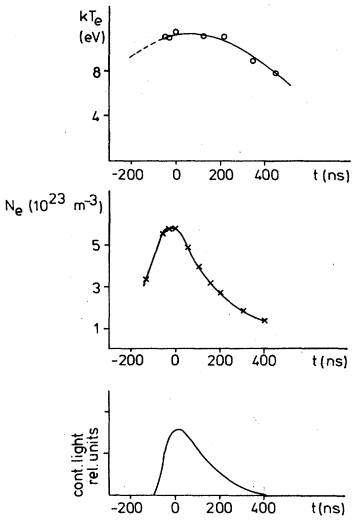

FIG. 2. The temperature (kT_e), electron density (N_e), and continuum light intensity as a function of time.

sivity as described in Chap. 5.4 of Ref. 10.

Most reliable results of the Abel inversion are obtained for the time of maximum compression because the density profile is then rather narrow and monotonically decaying in the radial direction. A typical example of the radial electron density distribution is given in Fig. 3. The column is about 2 cm in diameter, has steep gradients at the boundary but is flat for the inner 1 cm. The absolute value of N_e agrees within 5% with the value given by formula (1). The overall accuracy of both experiments together is estimated to be better than 10%. This confirms the validity of formula (1).

By shifting the wavelength of the monochromator to the center of P_α of He II in a similar way the distribution of the test gas during the discharge is obtained. The non-Abel-inverted distribution of the test gas is shown in Fig. 3 in comparison to the electron density distribution. The photon noise of the signal has not yet been smoothed out. It is obvious that the test gas is indeed concentrated at the center of the discharge as was expected for the gas-liner pinch. The gradients of the electron density at the boundary are so steep that the test gas emits light predominantly from a volume of constant density, i.e., as the linewidth of P_α is everywhere constant, the central line intensity represents also the He^+ density in the upper level of the line. A correction of a measured line shape with the actual density distribution is always within the thickness of the drawing ink. If the percentage of the test gas is increased with respect to the driver gas, the domain of the test plasma increases. But even for these cases a correction of the spectral lines was unnecessary.

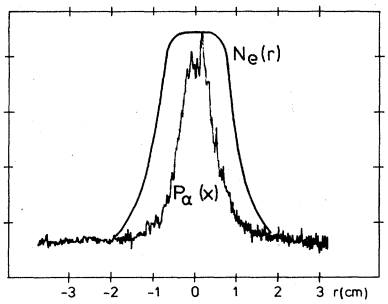

FIG. 3. The relative radial electron density distribution $N_e(r)$ and the recorded intensity distribution of the P_α line at the line center.

The emission profile of spectral lines from the driver gas—here, e.g., H_2—agrees very well with the electron density distribution. The only difference is a smaller decrease at the very boundary of the column.

The other important parameter of the plasma is the electron temperature. This value is derived from the line intensity ratios of C IV to C III. Figure 2(a) gives the results of this measurement. The maximum temperature is about 11 eV, i.e., a factor of 3 higher than in the experiment of Ref. 5. Following the expansion of the plasma, the temperature drops to 8 eV. For times before maximum continuum light emission, the line ratio gives no meaningful temperature because the ions have not yet achieved their equilibrium. For the determination of the temperature, the C III 4647.4-Å and C IV 4658.3-Å lines were selected because they are close to P_α as seen in the example of Fig. 4; so one spectrum yields both the electron density and the electron temperature at one instant of the discharge. To derive the electron temperature the C III and C IV lines were related via the Boltzmann relation to the lines treated by Griem[10] in Chap. 13. This procedure is valid because both the low-lying levels of C III and the high-lying level of C IV are in partial local thermodynamic equilibrium (PLTE) with the ground states of C III and C IV, respectively. For electron densities up to 1×10^{23} m^{-3} the corona model between the C III and C IV ions is applicable, as assumed by Griem. This assumption becomes somewhat questionable for the electron density $N_e=5\times10^{23}$ m^{-3}. In the other limit, Saha equilibrium holds for $N_e>5\times10^{25}$ m^{-3}. Since the experimental conditions are much closer to the corona model, we still use this model.

IV. LINE PROFILES OF P_α AND P_β OF He II

Line profiles of P_α ($\lambda=4686$ Å) and P_β ($\lambda=3203$ Å) are shown in Figs. 5 and 6. The P_α line is strongly excit-

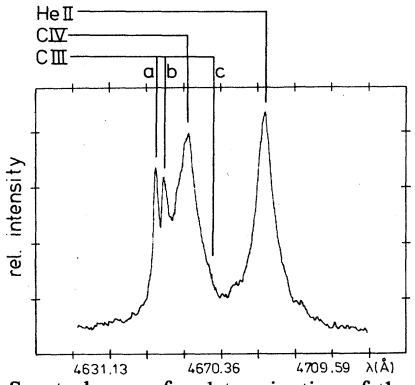

FIG. 4. Spectral range for determination of the temperature and electron density. He II: P_α (4686 Å). C IV: $5f\,^2F^o$–$6g\,^2G$ (4658.30 Å). C III: a,b, $3s\,^3S$–$3p\,^3P^o$ (4647.42, 4650.25, 4651.47 Å); c, $3s\,^3P^o_2$–$3p\,^3P^o_2$ (4665.86 Å). The contribution of the C IV 4646-Å line (5^2D-6^2F^o) and other members of the C III $^3P^o$–^3P transition have been taken into account.

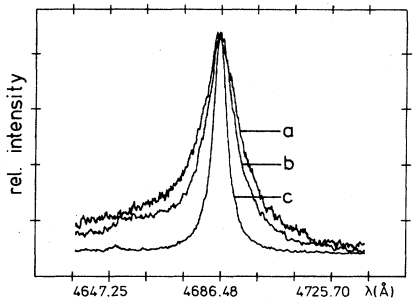

FIG. 5. The spectrum of the He II 4686-Å line at various electron densities: (a) 5.5×10^{23} m^{-3}, (b) 4.0×10^{23} m^{-3}, (c) 1.7×10^{23} m^{-3}.

ed for the interval of $-100\leq t\leq 500$ ns (compare Fig. 2). Before and after this interval emission from He I is dominant. The P_β line is less intense both because of the lower oscillator strength and because of the larger Stark broadening. In the wing, where the photon noise of the continuum light becomes comparable with the line intensity, details of the line cannot be interpreted.

The first-order effect of the action of ions and electrons on the spectral lines is a symmetric broadening which is therefore investigated at the outset. For the broadening of P_α and P_β, theories of Griem and Shen,[9] Kepple,[11] and, within the framework of the unified theory, Greene[12] have been evaluated; all theories give different results. The strongest broadening is predicted by Kepple whereas the smallest effect is calculated by the unified theory. For electron densities of $10^{22}\leq N_e\leq 10^{23}$ m^{-3}, the line broadening has been compared to the measurements of Ref. 5. The empirical results found there coincide best with the theory of Griem and Shen.[9]

Experimental results concerning the broadening of He II lines published up to 1979 have already been discussed by Soltwisch and Kusch.[13] Almost all these results are best approximated by the first prediction of Griem and Shen,[9] and in their recent work Bernard *et al.*[14] confirm these conclusions. They do not discuss the asymmetry of the lines.

In our investigations we performed a consistency check of P_α and P_β and calibrated the broadening against the absolutely measured continuum light emission of the plasma. As discussed above the results are consistent within 5%. In Fig. 7 the measured full half-widths of the P_α and P_β lines as a function of time are shown. In Fig. 8

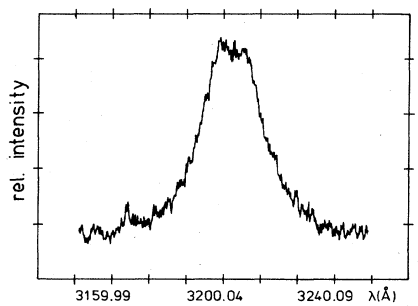

FIG. 6. Spectrum of the He II 3203-Å line at an electron density of 3.2×10^{23} m^{-3}.

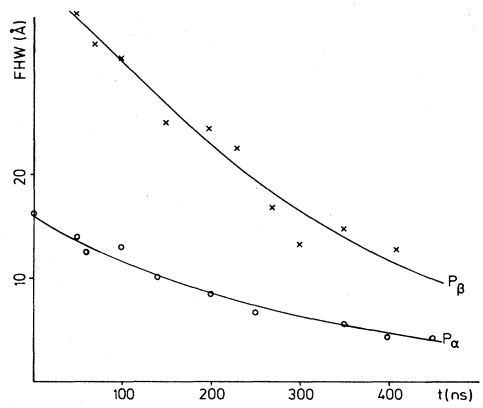

FIG. 7. Full half-widths of the P_α and P_β lines as a function of time.

the half-widths of the P_β line are presented for several values of the electron density. In this figure other experimental results and theoretical predictions are also presented. As one can see, the experimental results agree very well with the results of Griem and Shen for the electron density range between $(2-6)\times10^{23}$ m^{-3}. The best agreement would be achieved for a straight line given by a function:

$$N_e=4.1(\Delta\lambda_{\mathrm{FWHM}}^{1.35})\times10^{22}\ \mathrm{m}^{-3}\ . \tag{2}$$

The discrepancy for the electron density derived from P_α and P_β according to Kepple amounts up to 15% where P_α yields the higher value. For the unified theory no data were published for P_β.

A detailed analysis shows that the P_α and P_β lines are not only broadened by the plasma but are also asymmetric; for P_α the intensity at shorter wavelengths is enhanced, for P_β the blue side intensity is only stronger near the center while at the wings the red side dominates. The P_β blue side shoulder is about 5% higher than the red shoulder. This asymmetry is usually attributed to the quadrupole effect[15,16] whereas the shift is either attributed to electron collisions or to the plasma polarization shift. To obtain quantitative information about higher-order perturbations on spectral line shape, the asymmetry $\Delta\beta$ is calculated as a function of the spectral distance $\Delta\alpha$ from the line center. To eliminate first-order density effects, $\Delta\alpha$ and $\Delta\beta$ are normalized to the quasistatic Holtsmark field strength F_0:

$$\Delta\alpha=\frac{1}{F_0}\frac{1}{2}(\lambda_r-\lambda_b)\ , \tag{3}$$

$$\Delta\beta=\frac{1}{F_0}\frac{1}{2}(\lambda_r+\lambda_b-2\lambda_0)\ . \tag{4}$$

The different symbols are explained in Fig. 9. In calculations of $\Delta\alpha$ and $\Delta\beta$ the trivial asymmetry of the lines which is proportional to ω^4 has been subtracted. Asymmetries from a different population of the Stark sublevels are negligibly small at the given electron temperature. For the following data the P_α line was analyzed from the intensity range from 90—10% and the P_β line from 75—20% of the maximum intensities. The far wings of

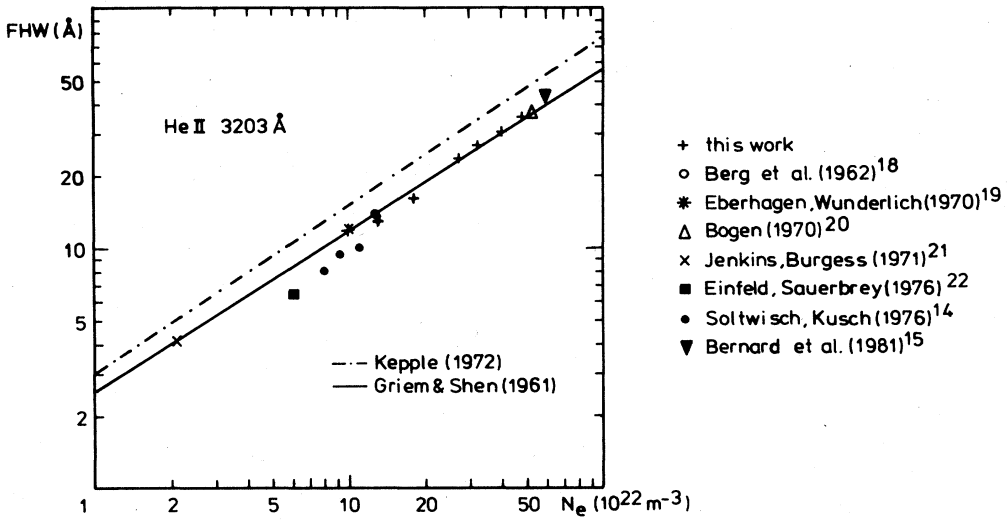

FIG. 8. Full half-widths of the P_β (3203 Å) line vs electron density. +, this work; o, Ref. 17; *, Ref. 18; Δ, Ref. 19; ×, Ref. 20; ■, Ref. 21; ●, Ref. 13; ▼, Ref. 14.

the lines are omitted because of the strong continuum background light. The central wavelength λ_0 is determined from low-density conditions, i.e., from spectra of about 500 ns after the maximum compression, and from calibration spectra. The accuracy amounts to <0.1 Å. For an unshifted symmetric spectral line $\Delta\beta=0$ at all spectra positions while $\Delta\beta=$const for a purely shifted line; blue-shifted parts of a line lead to a negative sign of $\Delta\beta$ and the red-shifted parts to a positive sign. For symmetric lines $\Delta\alpha$ corresponds to the parameter commonly used in line-broadening theory.

Figures 10 and 11 represent the deviations from symmetry at P_α and P_β for different electron densities. To clarify the effect, the axes $\Delta\alpha$ and $\Delta\beta$ are not on a common scale. The experimental values of P_α are an average of different discharges. To obtain a better spectral resolution, the central part of P_α is recorded in second order of the spectrograph. The figures indicate that the asymmetry increases rapidly with increasing electron density.

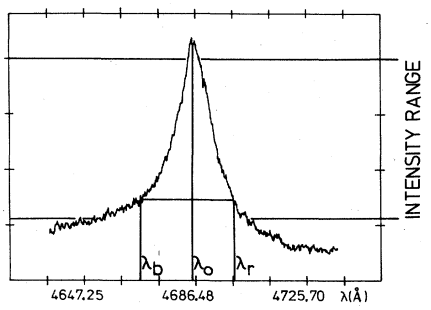

FIG. 9. Definition of asymmetry parameter of a spectral line. The analyzed intensity range of the P_α line for the asymmetry study is shown.

The central part of P_α is slightly red shifted while the bulk shows a blue shift. As already seen qualitatively in Fig. 6, P_β shifts in just the opposite direction; the magnitude, however, is about a factor of 5 smaller than for P_α. The scatter of the experimental values is larger for P_β than for P_α because of the weakness of the line. To get a better feeling for the reproducibility of the effect the data distribution of the asymmetry is drawn for three different events. Each individual discharge gives nearly the same tendency.

Griem[4] calculates the influence of distant electron collisions and of the quadrupole effect on the line profile of different He II lines. The collisions give rise to a red shift of about $(\Delta\lambda/\lambda)_c=3.7\times10^{-5}$ for P_α and 6.5×10^{-5} for P_β at electron densities of 1×10^{23} m^{-3} and $T_e=5.7\times10^4$ K. The value changes linearly with density but is only little affected by the temperature.

The shifts due to the quadrupole effect are given as averages over parts of the line profile between $\frac{1}{2}$, $\frac{1}{4}$, and $\frac{1}{8}$ intensity points again for $N_e=1\times10^{23}$ m^{-3} and $T_e=4\times10^4$ K. The values for P_α and P_β are

	P_α	P_β
$10^5(\Delta\lambda/\lambda)_q(\frac{1}{2})$	−0.5	−1.5
$10^5(\Delta\lambda/\lambda)_q(\frac{1}{4})$	−0.8	−2.4
$10^5(\Delta\lambda/\lambda)_q(\frac{1}{8})$	−1.2	−3.0

The minus sign indicates a blue shift. The average shift for the quadrupole effect is defined as

$$\langle\omega_q\rangle=\int_{-\Delta\omega_0}^{\Delta\omega_0}\omega L_q(\omega)d\omega\ . \tag{5}$$

Unfortunately, this mean is not constant for a symmetric but shifted line profile as for instance $\Delta\beta$ is. In the limit that $\Delta\omega_0$ is much larger than the shift δ, $\langle\omega\rangle$ yields

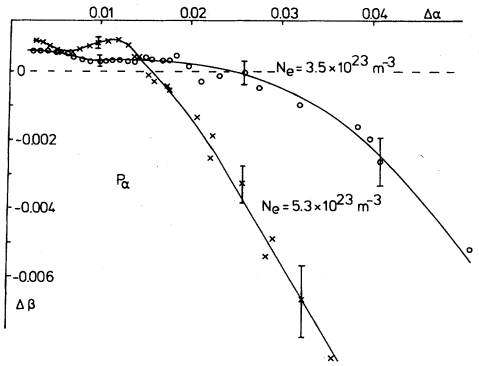

FIG. 10. The asymmetry of the He II 4686-Å line. The curve represents a spline fit of the measured data. The errors of the data are estimated to 10% on the line wing because of the photon noise, near the line center, the errors caused from the noise can be neglected.

$$\langle\omega\rangle = \delta 2 \int_0^{\Delta\omega_0} L(\omega)d\omega \ . \tag{6}$$

For the evaluation of $\langle\omega\rangle$ for an asymmetric line which is additionally shifted it would be advantageous to have tabulated values of the asymmetric part. As this is not available we define, similarly to the quadrupole part, the average shift due to electron collisions,

$$\langle\omega_c\rangle = \int_{-\Delta\omega_0}^{\Delta\omega_0} \omega L_s(\omega-\omega_c)d\omega \tag{7}$$

and for the measured data

$$\langle\Delta\beta\rangle = \int_{-\alpha_0}^{\alpha_0} \Delta\beta L_s(\alpha)d\alpha \ . \tag{8}$$

Here $L_{s(}\omega)$ and $L_s(\alpha)$ are the symmetric line-shape functions as, e.g., tabulated by Griem. The average shifts of the $\frac{1}{2}$, $\frac{1}{4}$, and $\frac{1}{8}$ intensity points are summarized in Table I. The table is split into three sections, two for P_α ($N_e = 3.5\times10^{23}$ and 5.3×10^{23} m^{-3}) and one for P_β ($N_e = 4.4\times10^{23}$ m^{-3}). The columns state the average line shifts due to electron collisions, those due to the quadrupole field produced by ions, the sum of both, the observed mean shift, those due to the plasma polarization (see, e.g., Ref. 22), and the extrapolated values of Ref. 5. The average is taken over the range where the intensity is $\frac{1}{2}$, $\frac{1}{4}$, and $\frac{1}{8}$. The absolute values for P_α agree, especially at low densities, very well with the theoretical predictions. At higher densities the central value fits well while the outer part of the line is less well predicted. The deviation from the theory manifests itself most strongly by the change of the sign. The experimental data for P_β are less reliable than for P_α; but also it seems here that the sign of the shift is predicted wrongly. Comparison of Figs. 10 and 11 with Table I reveals that the average over the line sections smoothes out the details of the shift. The weighting with $L(\omega)$ strongly favors the line center. Therefore the good agreement of the central values of $\Delta\lambda_{1/2}$ (only for P_α) indicates that the electron collision process dominant in the line center is well described within the experimental errors. The quadrupole effect, however, seems to be stronger than predicted on the line wings. A qualitative picture of the manifestation of the combined quadrupole and quadratic Stark effect as treated by Sholin[15] is given in Fig. 12. The strongest Stark components are plotted as a function of the difference of parabolic quantum numbers of the upper and lower atomic levels corresponding to the electron densities $N_e = 1\times10^{23}$, 5×10^{23}, and 1×10^{24} m^{-3}. In this simple model the electron density determines both the electric field strength resulting from the distance to the next ionic neighbor and the parameter

$$\frac{a_0}{R} = \frac{a_0}{(\frac{4}{3}\pi N_e)^{1/3}} \ . \tag{9}$$

It is obvious from Fig. 12 that the quasistatic Stark components are shifted to the blue side at the line center while they are red shifted on the wing. The components are slightly stronger for longer wavelengths than for shorter ones; this however, is only a smaller effect. To judge the final line profile it has to be borne in mind that the Stark components represent δ functions which are broadened by the impact of the electrons. Therefore, on the strongest part of the line the line profile is lifted in the blue, because the separation of the components becomes smaller in contrast to the red side. At the far red wing the intensity should be higher, because the corresponding blue components are shifted away. The asymmetry of the P_α line is apparently more pronounced than would be expected by the mean shift of the components. The measured values (Figs. 5 and 10) are in good qualitative agreement with the features in Fig. 12. The bulk of the line is indeed blue shifted. A shift of the P_α due to plasma polarization is calculated to be in the order of the observed shift in the line center. There are, however, doubts whether the plasma polarization shift of the Debye model is consistent with the measurement.[4] The line shift observed in our experiment compared to the one done by Pittman and Fleurier[5] yields consistent results if one assumes that the shift is not strongly temperature dependent. This would, therefore, not favor the assumption that the shift is mainly determined by the plasma polarization.

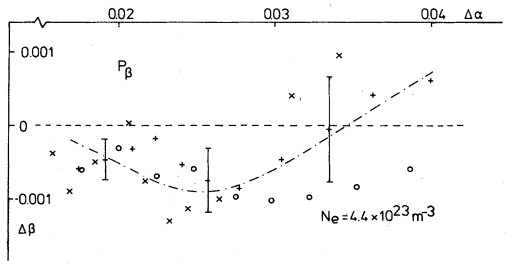

FIG. 11. The asymmetry of the He II 3203-Å line. The curve represents a spline fit of the measured data. In contrast to the error of the P_α investigation, the photon noise is higher for the whole line profile. In addition, in this picture data of three different discharges are shown. The limited reproducibility of the device increases the total error, which is thus estimated to 30%.

TABLE I. Comparison of the theoretical and experimental line shift of P_α and P_β at different ranges of the line profile. The measured values of Pittman *et al.* (Ref. 5) have been extrapolated from Fig. 7 of Ref. 5; $\delta\lambda = 2.1\times10^{-2}(\Delta\lambda_{\mathrm{FWHM}}^{1.2})$ Å. Here $\Delta\lambda_{\mathrm{FWHM}}$ is the full half-width of the P_α line in Å. The shift as a function of electron density is given by $\delta\lambda = 1.03\times10^{24}(N_e)$ Å. The electron temperature has been taken constant.

Range	Electrons[a] (Å)	Ions[b] (Å)	Total[c] (Å)	Expt. (Å)	Debye model (Ref. 6, in Å)	Extrapolated values (Ref. 5, in Å)	
$\frac{1}{2}$	0.28	−0.08	0.20	0.16	0.17	0.17	P_α
$\frac{1}{4}$	0.39	−0.13	0.26	0.20			$N_e = 3.5\times10^{23}$ m^{-3}
$\frac{1}{8}$	0.47	−0.20	0.27	0.20			$kT_e = 10$ eV
$\frac{1}{2}$	0.42	−0.12	0.30	0.29	0.26	0.25	P_α
$\frac{1}{4}$	0.59	−0.20	0.39	0.32			$N_e = 5.3\times10^{23}$ m^{-3}
$\frac{1}{8}$	0.72	−0.30	0.42	−0.10			$kT_e = 10$ eV
$\frac{1}{2}$	0.52	−0.21	0.31		0.30		P_β
				−0.3			
							$N_e = 4.4\times10^{23}$ m^{-3}
							$kT_e = 10$ eV

[a]Shift caused by electronic collisions.
[b]Shift caused by ion field gradients (quadrupole interactions).
[c]Sum of both (electrons and ions).

V. THEORY FOR THE BROADENING OF ISOLATED LINES

Estimates of the broadening by collisions of electrons start from the equation given by Baranger:[23]

$$W_{if} = \tfrac{1}{2} n \left[v \left(\sum_{i'} \sigma_{ii'} + \sum_{f'} \sigma_{ff'} + \int |f_i(\theta,\phi) - f_f(\theta,\phi)|^2 d\Omega \right) \right]_{\mathrm{av}} . \quad (10)$$

Here N is the perturber density, and v the electron velocity over which Eq. (10) has to be averaged. The $\sigma_{ii'}$ and $\sigma_{ff'}$ are the inelastic cross sections for collisional transitions to levels i,f from initial (i) and final levels (f), respectively, of the optical transition; f_i and f_f are elastic scattering amplitudes for the two states of the perturbed system. With Eq. (10) the difficulties for determining the linewidth are transferred to the calculation of the collisional cross section. The solution of this problem is generally very difficult if the inner structure of the atom is treated accurately (see Ref. 24). An approximation to the scattering process is given in Ref. 25; here the internal structure of the atom is neglected and only the large-scale electrostatic monopole and dipole potentials are retained. This procedure leads to the scattering cross section

$$\sigma_{if} = \frac{2\pi}{\epsilon \Delta E \sqrt{3}} f_{if} g_{\mathrm{eff}} , \quad (11)$$

where ϵ is the energy of the incoming electron, ΔE the energy gap of the atomic states under consideration, f_{if} the oscillator strength of the optical transition between the atomic states, and g_{eff} the effective Gaunt factor. This relation, which is valid only for allowed optical transitions, relates the photon cross section to the electron collision cross section. All problems arising from quantum mechanics are shifted to the transition probability and to the Gaunt factor. The interaction between the complicated atomic structure and the incoming electron is hidden in g_{eff}. Therefore, Eq. (11) is only meaningful if g_{eff} is a rather universal function, e.g., of ϵ but not of the specific atom, because otherwise g_{eff} would have to be determined for each atomic transition separately. For transitions caused predominantly by distant collisions, it is obvious that the specific atomic structure is less important. This condition is indeed met for collisions with neutral atoms as it can be estimated from the relevant impact parameter[26]

$$\rho = \frac{2n^2}{Z+1}\frac{\hbar}{mv} \approx \frac{2n^2 a}{Z+1}(E_H/kT)^{1/2} . \quad (12)$$

For the ion core charge $Z=4$ and $kT \approx E_H$ the dominant impact parameter is only 2 times higher than the Bohr radius of the excited state. So it is interesting to test experimentally how good the theoretical estimations can be applied to a triply ionized atom. Furthermore, as already pointed out, C IV is nearly hydrogenlike. This is important insofar as in all simpler estimations of the line-broadening, hydrogen wave functions are used. Corrections due to the quantum-defect method as introduced by Bates[27] are practically negligible.

The effective Gaunt factor commonly used is a combination of theoretical estimates and experimental fittings. For an optically allowed transition it can be written as[28]

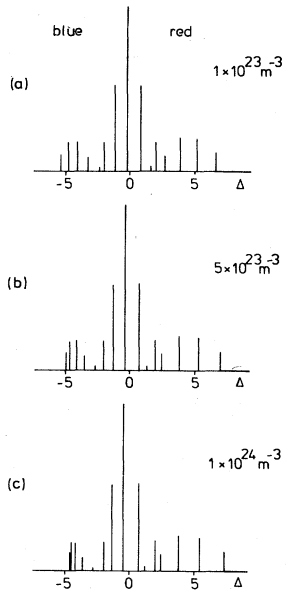

FIG. 12. Strongest Stark components of P_α for different electric field strengths as a function of the difference of parabolic quantum number of the upper and lower atomic niveaus.

$$g_{\text{eff}}=\bar{g}_0+A\ln[1+B(x-1)] \tag{13}$$

with the fitting parameters g_0, A, and B; $x=\epsilon/\Delta E_{ij}$. For present calculations we use the data of Dimitrijević and Konjević,[29] especially formulas 7—10. The broadening w essentially consists of three parts, namely, of a broadening due to interactions with the neighbor terms $(l-1)$ and $(l+1)$ and due to inelastic collisions $\Delta n\neq 0$.

There exists another more recent calculation of Griem[1] (Eqs. 526 and 515) which uses estimates similar to those from Ref. 29. A difference, however, is the choice of the Gaunt factor. There are also more effects considered which contribute to the broadening: these effects are "strong collisions," i.e., close collisions and higher multipoles in the quantum-mechanical expansion.

The calculations of C IV show a stronger broadening according to Griem[1] (Eq. 526) than the semiempirical calculations of Ref. 29 because more effects are taken into account. In Tables II and III we will compare the experimental results to Griem,[1] to the semiclassical calculation of Dimitrijević and Koniević,[29] and, additionally, we will give the relative contribution of the different collision processes for these values.

VI. RESULTS AND DISCUSSION OF THE BROADENING OF C IV

All experimental characteristics such as density distribution, test gas distribution, and temperature remain unchanged compared to the He measurements. Figure 4 shows a collection of He II, C III, and C IV lines which allows a determination of the density and temperature during one exposure. This set of lines proves to be very useful also for the following investigations, for it allows a transition standard from the broadening of the He II P_α line to the C IV $5F,5G$-$6G,6H$ line. The discharge conditions shortly after maximum compression are such that the C III lines in Fig. 4 are so weak that the broadening of the C IV $5F,5G$-$6G,6H$ line is not disturbed. The linewidth amounts to about 21 Å so that uncertainties from the instrumental broadening are negligible.

We have measured C IV lines which are wide and intense enough for a meaningful investigation. The requirement of the width arises from the resolution of the spectrometer which amounts to about 0.17 Å for the vuv monochromator and 1 Å caused by the OMA II system in the first order of the spectrum. Lines with an intensity of less than half the continuum intensity were excluded because the photon noise became too large for a reliable interpretation of the line broadening. Finally, the measurements were restricted to lines with different upper quantum numbers. A survey of the lines actually investigated is shown in the Grotrian diagram of Fig. 13. The lines can be divided into different groups: the transitions from $n\leq 4$ and $n=5,l=1$ correspond to isolated lines while the levels $5F,5G$, $6D,6F,6G,6H$, and $7D,7F,7G,7H,7I$ are degenerate because the line splitting is smaller than $\hbar\omega_{pe}$.

The Li-like C IV system is a doublet system, i.e., each line consists of three components with $\Delta J=\pm 1$ and 0. The transition with $\Delta J=0$ is weak and can often be neglected for the analysis of the data. The line strength of the components is related to

$$R^2_{\text{line}}=(2J_i+1)(2J_f+1)W^2(SJ_iL1;L_iJ_f)\ , \tag{14}$$

$$R^2_{\text{mult}}=(2L_i+1)(2L_f+1)W^2(L_cL_il_f1;l_iL_f)\ . \tag{15}$$

The index c indicates the core, the other notation has the usual meaning. $6j$ symbols, which are related to the Racah coefficients W, are summarized, e.g., in Landolt-Börnstein.[30]

The components of the doublet system are close together so that only some transitions are resolved by our monochromator ($3S$-$3P$, $3P$-$4S$). But even though these lines

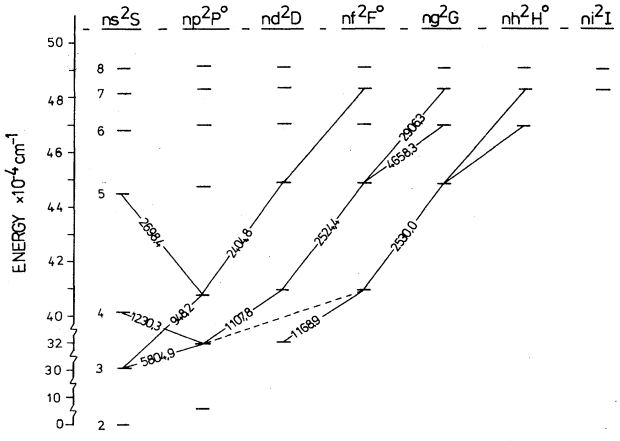

FIG. 13. Grotrian diagram of the C IV ion. The studied transitions are indicated by solid lines. The dashed line will be discussed separately.

TABLE II. Comparison of experimentally observed and theoretically calculated line broadening of C IV. DK denotes effective Gaunt-factor approximation as proposed by Ref. 29 and G stands for Griem (Ref. 1). FHW stands for full half-width. $N_e = 5\times10^{23}$ m^{-3}, $T_e = 10$ eV. Static represents the quasistatic average.

Term	λ (Å)	λ (Å) FHW expt.	λ (Å) FHW G	$\frac{\lambda_{expt}}{\lambda_G}$	λ (Å) FHW DK	$\frac{\lambda_{expt}}{\lambda_{DK}}$	λ (Å) FHW static
3s-3p	5801/5811	2.8	2.6	1.08	1.8	1.55	
3p-4s	1230	0.58	0.28	2.07	0.2	2.9	
3s-4p	948.1	0.4	0.19	2.1	0.16	2.5	
3p-4d	1107.6	0.53	0.29	1.83	0.23	2.3	
3p-4f*	1106.5	0.35	0.12	2.92	0.12	2.92	
3d-4f	1169	0.4	0.12	3.3	0.12	3.3	
4p-5s	2698	5.4	4.4	1.23	3.7	1.46	
4p-5d	2405	10.0	4.4	2.27	4.0	2.5	
4d-5f	2524.4	8.4	4.5	1.87	3.8	2.21	{13}
4f-5g	2530	4.2	2.0	2.1	1.6	2.63	{13}
5f-6g, 5g-6h	4658	21	⟨18⟩	1.17	⟨13.5⟩	1.56	{55}
5f-7g, 5g-7h, 5d-7f	2906	33	⟨19.5⟩	1.69	⟨15.5⟩	2.12	{47}

TABLE III. The absolute value of the line broadening in Å and the relative contributions of the different processes in %.

			Griem				Dimitrijević and Konjević			
		Å	$W(l+1)$	$W(l-1)$	W(inel)	W(sc)	Å	$W(l+1)$	$W(l-1)$	W(inel)
3s-3p	5801/5811 *i*	1.4	25	13	4	12	0.95	31	18	4
	f	1.2	33		3	10	0.84	44		3
3p-4s	1230 *i*	0.22	61		3	14	0.18	80		2
	f	0.06	10	5	2	5	0.04	11	6	1
3s-4p	948.1 *i*	0.16	47	20	4	13	0.14	62	24	1
	f	0.03	12		1	3	0.02	12		1
3p-4d	1107.6 *i*	0.24	38	27	5	13	0.20	50	35	2
	f	0.05	8	4	1	4	0.03	8	4	1
3p-4f*	1106.5 *i*	0.07		34	9	16	0.09		70	5
	f	0.05	19	11	3	8	0.03	15	8	2
3d-4f	1169 *i*	0.08		39	10	18	0.10		78	5
	f	0.04		15	6	12	0.02		13	4
4p-5s	2698 *i*	3.1	57		3	11	2.6	68		2
	f	1.3	16	7	1	5	1.1	22	8	0
4p-5d	2405 *i*	3.4	40	25	3	9	3.1	46	28	3
	f	1.9	13	5	1	4	0.9	16	6	1
4d-5f	2524.4 *i*	3.2	24	32	5	11	2.7	28	38	5
	f	1.3	13	9	2	4	1.1	17	11	1
4f-5g	2530 *i*	1.6		42	15	24	1.1		54	15
	f	0.37		11	3	5	0.5		29	2
5f-6g	*i*	20	19	28	6	11	17	23	34	8
	f	11	12	16	3	5	9.3	14	19	2
	4658			⟨18⟩					⟨13.5⟩	
5g-6h	*i*	11		31	15	21	7.5		43	24
	f	5.5		17	6	10	3.7		26	7
5d-7f	*i*	20	35	31	4	10	19	40	35	6
	f	5.0	10	7	1	2	4.5	11	7	1
	2906			⟨19.5⟩					⟨15.5⟩	
5f-7g	*i*	17	30	34	6	11	15	34	38	9
	f	4.2	6	9	1	3	3.6	8	10	1
5g-7h	*i*	13	23	36	11	16	11	28	43	18
	f	2.1		7	3	4	1.4		9	2

are very close and the separations smaller than the half-width, these doublets are mostly "isolated" because the wave function of the two J components do not mix under the influence of the electrical field in contrast to the case where levels with adjacent l-numbers are close together. So the line-broadening data are obtained by folding two or more components with given wavelength separation, given intensity ratio of the individual components, and by comparing these calculations to the experimental data. Additionally it is assumed that the broadening from the two J components of the same (n,l,L) state are equal. Examples of the shape of some lines are given in Figs. 14 and 15, for more "isolated" lines, and in Figs. 16 and 17 for lines from degenerate states. Figure 17 shows the line shape of the $\Delta n=2$ transition $5D,5F,5G$-$7F,7G,7H$. Because the $n=7$ level is nearly degenerate we obtain a contour like that of hydrogen lines, as has already been pointed out. Also, the intensity of the blue line shoulder is about 10% higher than the red one, as has been measured for hydrogenlike atomic systems. The details of some lines will be discussed later.

A summary of the line-broadening data for the different lines is given in Table II. The first column shows the terms of the atomic transition, the second one gives the corresponding wavelengths. The third column contains the full half-width of the lines derived from the measurements. All values are for an electron density of $N_e=5\times10^{23}$ m^{-3} and a temperature of $kT_e=10$ eV. The apparatus profile and the Doppler width contribution have been deconvolved. These experimental data are compared to the theory of Griem (Eq. 526 of Ref. 1) and the

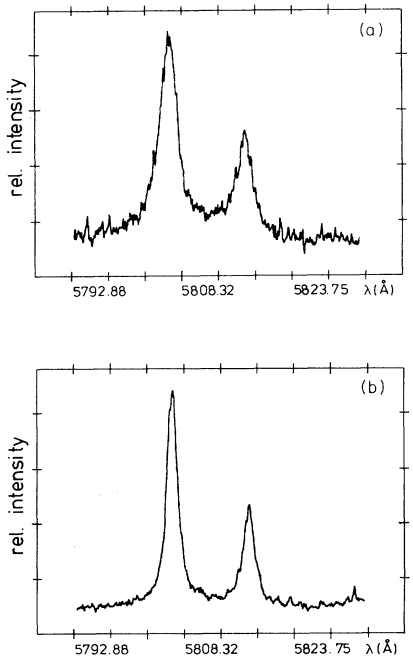

FIG. 14. Line shapes corresponding to the well-isolated transition $3S$-$3P$ at two different electron densities of the plasma: (a) $N_e=5.0\times10^{23}$ m^{-3}, (b) $N_e=2.6\times10^{23}$ m^{-3}. The typical doublet structure of a Li-like spectrum is evident.

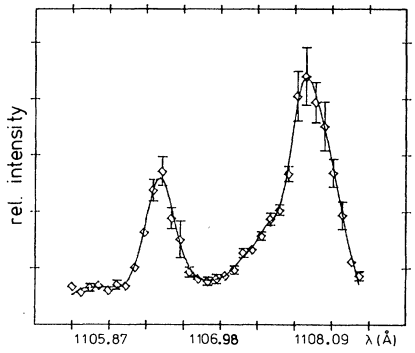

FIG. 15. Line shape of the vuv transitions $3P$-$4D$ for an electron density $N_e=3.7\times10^{23}$ m^{-3}. The line at the wavelength 1106.5 Å corresponds to the forbidden transition $3P$-$4F$. The second component of the $3P$-$4D$ transition is very weak.

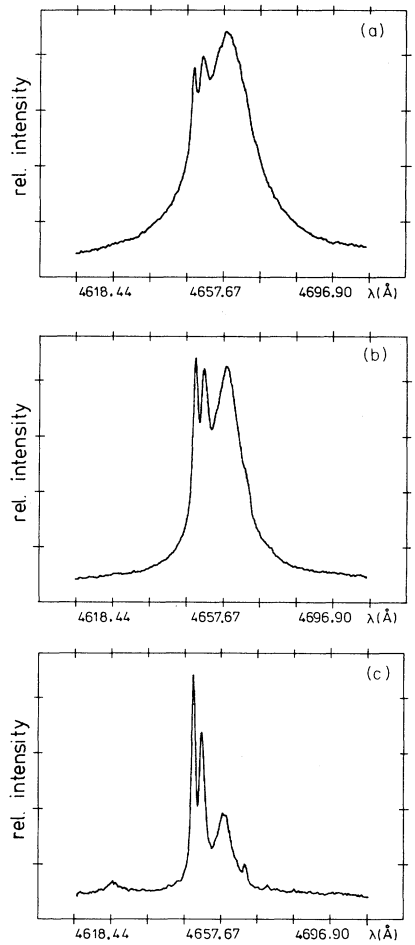

FIG. 16. The spectrum of C III and C IV in the wavelength range 4605–4710 Å recorded at conditions with various electron densities: (a) $N_e=5.0\times10^{23}$ m^{-3}, (b) $N_e=3.1\times10^{23}$ m^{-3}, (c) $N_e=1.5\times10^{23}$ m^{-3}. The narrow lines at 4647.4, 4651.5, and 4665.9 Å correspond to the C III spectrum, the broad line arises from C IV transitions $5F$-$6G$ and $5G$-$6H$. The intensity ratio of C IV to C III lines was utilized for determining the temperature of the plasma.

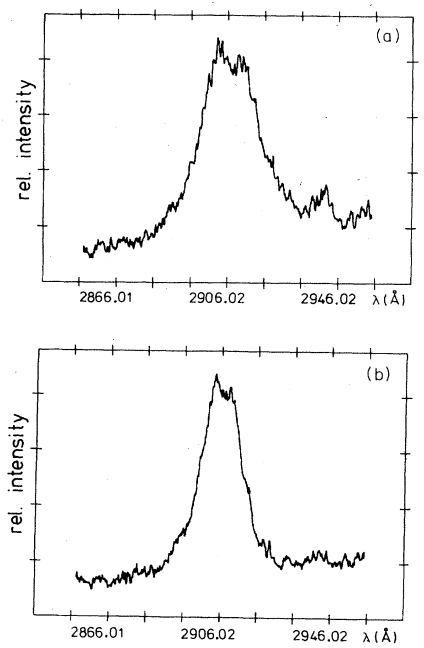

FIG. 17. Line shapes for the degenerate transition $5D,5F,5G$-$7F,7G,7H$ at electron densities (a) $N_e=4.5\times10^{23}$ m^{-3} and (b) $N_e=2.6\times10^{23}$ m^{-3}. The characteristic central dip for hydrogenlike transitions with $\Delta n=2$ is evident.

effective Gaunt-factor theory (Eqs. 6—10, Ref. 29). In addition, we quote the ratio between the experimental and theoretical values. The last column, finally, gives the estimate of quasistatic line broadening according to Griem:[1]

$$\omega\approx(12Z_p\hbar/Zm)(n_i^2-n_f^2)N_p^{2/3} . \quad (16)$$

The cutoff parameter needed for the Gaunt factor used for both theories is

$$\omega_c=\max\{\,|\omega_{l,l'}|\,,\omega_{pe},\omega_F,\Delta\omega_i\} . \quad (17)$$

Here $\omega_{l,l'}$ is the frequency separation between l,l' levels, ω_{pe} is the plasma frequency, ω_F is the fine-structure splitting and $\Delta\omega_i$ is the ion splitting. In our case for high principal quantum numbers $\hbar\omega_{pe}$ becomes larger than $\hbar\omega_{l,l'}$. If the cutoff at the Debye sphere were neglected, the theoretical data would become slightly higher at high l values than for the transitions from S or P levels.

The comparison between theory and experiment reveals that the theory predicts a broadening of the lines that is systematically smaller than that observed. On the average, the experimental values are 2.0 times higher than the theory of Griem and 2.4 times higher than the effective Gaunt-factor approximation; this average is taken only for the isolated lines. A further calculation performed by Sahal-Bréchot[31] for the half-width of the C IV line $3D$-$4F$ yields a higher discrepancy between the theoretical and the experimental values than the theories mentioned above. The only transition well predicted is the $3S$-$3P$ line. This transition has also been measured by Bogen[32] and El-Farra and Hughes.[33] If we take into account the slightly different plasma parameters, we find a good agreement for the half-width and the intensity ratio of the two lines (5801 and 5811 Å) according to our measurement.

A good agreement between theory and experiment seems to hold for the lines arising from $n=6$ and 7; this agreement, however, is only formal because these lines are no longer isolated as assumed in the theory. The values in the angle brackets are an average over the components of the line weighted with their intensities.

The degeneracy of the levels $n^*>6$ is consistent with the theoretical estimates (see Ref. 1, Chap. II, Sec. 3f). The width predicted by Eq. (16) overestimates, according to Griem, the width of low series members. Additionally, the hydrogenlike approximation of Eq. (16) is questionable because in this case the S and P levels are not degenerate, i.e., parabolic quantum numbers are no longer good quantum numbers. Therefore, no simple theory is valid for the transition from $5F,5G$; $6F,6H$; $7F,7G,7H,7I$; and so on.

A more detailed analysis of the different effects leading to the line broadening is given in Table III. There the results of the new calculation of Griem[1] and the results obtained according to the effective Gaunt approximation are presented. The first column gives again the transition, the second the wavelength of the lines. In the next column the total half-width (in Å) and the contribution to the half-width (in %) of the upper (i) and lower (f) levels are quoted. The contributions of different collision effects in relative units are listed: $W(l+1)$ is caused by collisional transitions to the neighboring level $(l+1)$ of the same principal quantum number and $W(l-1)$ by collisional transitions to the level $(l-1)$; W(SC) means broadening by strong collisions, i.e., by close collisions, and finally, W(inel) summarizes all collisional transitions to levels $\Delta n\neq0$. The dominant effect of the line broadening arises from the upper energy level; according to Eq. 526 of Ref. 1 the broadening increases with $(n^*)^2[(n^*)^2-l_>^2]$. Within each nondegenerate level the largest cross section is due to collisions with the level $(l+1)$. On the average the collisional cross section to the level $(l-1)$ is about 30% smaller. The broadening due to "strong collisions" amounts to 20%. This effect is neglected in the effective Gaunt approximation and therefore the broadening there is smaller. The inelastic collisions to levels $\Delta n\neq0$ are small in most cases.

For the transitions $5F,5G$-$6G,6H$ and $5D,5G,5F$-$7G,7H,7F$ we have also calculated the broadening of each component and averaged according to the weight of the transition probability. As the transition probability is larger for higher l-numbers, the mean value is shifted, e.g., to the $5G$-$6H$ or to $5G$-$7H$ transitions, respectively.

If additionally the corrections for ion broadening of isolated lines are taken into account (compare Ref. 1; Chap. II, Sec. 3f) the discrepancy between experimental and theoretical results is decreased. Table IV gives the corrections due to the quadratic Stark effect and the recalculated ratios of experimental to theoretical broadening data for the different lines. The mean deviation between observed and calculated data is reduced to a factor 1.5 (Griem) and 1.8 (Dimitrijević), respectively. The broadening from $n=5$ is predicted very well while the broadening

TABLE IV. Corrections due to ion broadening. The values are derived from Eqs. 224—226 of Griem (Ref. 1). See there also for the definitions. For ionized emitters the value of $0.75R$ is replaced by $1.2R$ [see discussion of formula 4-9 of Griem (Ref. 10)]. For all other transitions $A > 1$.

	A	$\frac{w_{\text{tot}}}{w}$	$\frac{\lambda_{\text{expt}}}{\lambda_G}$	$\frac{\lambda_{\text{expt}}}{\lambda_{\text{DK}}}$
$4s$-$3p$	2.56×10^{-2}	1.03	1.05	1.5
$4p$-$4s$	4.8×10^{-2}	1.06	2.0	2.7
$3s$-$4p$	7.8×10^{-2}	1.1	1.9	2.3
$3p$-$4d$	0.39	1.48	1.2	1.6
$3d$-$4f$*	0.61	1.75	1.9	1.9
$4p$-$5s$	6.5×10^{-2}	1.08	1.1	1.4
$4p$-$5d$*		1.86	1.2	1.3

corrections for $n \leq 4$ change only slightly. The asterisks in Table IV indicate that the value of A is already greater than 0.5 where the approximation becomes invalid. Quadrupole effects are negligible for all lines discussed in this context.

The 1106.5-Å line

The line at $\lambda = 1106.5$ Å as shown in Fig. 15 is not mentioned in standard wavelength tables,[34–36] so its classification was difficult. Extensive tests assured, however, that the line did not arise from other gas contributions; the time behavior clarified additionally that the transition belongs to the C IV system.

From the energy difference it would be consistent to attribute the line to the transition $3P$-$4F$ which is dipole forbidden. Therefore, we carefully studied the literature about beam-foil excitation[37] of C IV ions. Besides the doublet system there also exists a quartet system which is usually weak in plasmas. No transition explains the observed line, so that the $3D$-$4F$ transition remains the most probable candidate.

There are, on the other hand, indications which confirm our assumption: The observed linewidth of 0.35 Å is consistent with the width of $3D$-$4F$ of 0.4 Å but not, e.g., with the width of the transition $3P$-$4D$ of 0.53 Å.

Though the transition $3P$-$4F$ is forbidden for isolated ion lines, it can become allowed in dense plasma because the quasistatic electric field starts to mix the wave functions. According to Eqs. 70—75 of Ref. 1 the appropriate matrix eigenvalue problem is written as

$$\begin{bmatrix} E_{4D}-E_i & U \\ U & E_{4F}-E_i \end{bmatrix} \begin{bmatrix} C_{4Di} \\ D_{4Fi} \end{bmatrix} = 0 \tag{18}$$

with

$$U = U^{n,l-1,m}_{n,l,m} = -\frac{KnF}{Z_0}\left[\frac{(n^2-l^2)(l^2-m^2)}{4l^2-1}\right]^{1/2} \tag{19}$$

and $K = 0.0640$ cm^{-1} kV cm (see Ref. 34).

The ratio of the coupling coefficients C gives the ratio of the allowed line to the forbidden line

$$I_{3P\text{-}4F}/I_{3P\text{-}4D} = |C_{4F_1}/C_{4D_1}|^2 = |C_{4D_2}/C_{4F_2}|^2 . \tag{20}$$

For $N_e = 3.5\times10^{23}$ m^{-3} this yields

$$I_{3P\text{-}4F}/I_{3P\text{-}4D} = \begin{cases} 0.27 \text{ for } |m| = 0 \\ 0.26 \text{ for } |m| = 1 \\ 0.19 \text{ for } |m| = 2 \\ 0 \text{ for } |m| = 3, \end{cases}$$

where m is the magnetic quantum number. On the average the observed line intensity satisfies these data.

The only weak point in these considerations is that mixing of wave functions is also associated with a shift of the energy levels. The electrostatic field causes both the "forbidden line" and a shift between allowed and forbidden lines. For densities of $N_e = 5\times10^{23}$ m^{-3} the energy shift amounts to 36, 32, 22, and 0 cm^{-1} for the magnetic quantum numbers $m = 0$, 1, 2, and 3. A slight shift of the two lines $3P$-$4D$ and $3P$-$4F$ is indeed observed in the experiment but its value is too small by at least a factor of 2. We think that we can give a more satisfying answer on the origin of the line at 1106.5 Å when we are also able to use the OMA II system in the vuv spectral region.

VII. CONCLUSIONS

We have performed spectral line measurements of He II and C IV in a gas-liner pinch. This device is optimized to produce a homogeneous plasma for spectroscopic purpose. The main advantage of the device is that the interesting lines are only emitted from a volume close to the axis, where electron density and temperature gradients are small. This allows an accurate determination of the local line profile without a tedious Abel inversion.

The electron density was determined by measuring the absolute continuum and the broadening of the P_α line of He II. The small and handy light source yields an electron density of 5×10^{23} m^{-3} and a temperature of $kT \approx 10$ eV.

The P_α and P_β spectral lines of He II are analyzed with respect to line asymmetries as a function of electron density. At the relatively high plasma temperature and density, the line profile differs from results obtained by Pittman and Fleurier[5] for a cooler plasma. The gross shift of the P_α line changes sign and the line asymmetry becomes more pronounced. The different results may be explained by a combination of electron collisions and by the quadru-

pole effect. The latter effect seems more pronounced at the line wing.

The broadening of the C IV lines is related to the measured electron density. The results are compared with the effective Gaunt-factor approximation theory of Dimitrijević *et al.* and the theory of Griem, taking into account some more effects. It is found that the observed broadening is about a factor of 1.5 higher than the calculated one. The theory of Griem gives a better agreement with the observations than the effective Gaunt-factor approximation. There still remains, however, a gap which is well above the limit of error. The lithiumlike atomic system can be described fairly well by hydrogenlike wave functions, and additionally some of the energy levels are not yet degenerate; so it is expected that this system fits best the assumptions used in the theories. We find, however, a systematic deviation from the experimental values, and it has to be concluded that either the Gaunt factors are estimated too small or that important effects (e.g., ion broadening) have been neglected. It seems important, therefore, to extend similar investigations to heavier lithiumlike ions.

ACKNOWLEDGMENTS

The authors appreciate helpful discussions with H.-J. Kunze. This work was supported by Sonderforschungsbereich 162 (Plasmaphysik Bochum/Jülich).

*Present address: Brown Boveri Research Center, CH-5401 Baden, Switzerland.

†Present address: Kernforschungsanlage Jülich GmbH, D-5170 Jülich, Federal Republic of Germany.

‡Permanent address: Institute of Physics, Teacher's Academy, PL-45-052, Opole, Poland.

[1]H. R. Griem, *Spectral Line Broadening by Plasmas* (Academic, New York, 1974).

[2]K. Yamamoto and H. Narumi, Prog. Theor. Phys. **64**, 436 (1982).

[3]K. Yamamoto, J. Phys. Soc. Jpn. **49**, 730 (1980).

[4]H. R. Griem, Phys. Rev. A **27**, 2566 (1983).

[5]T. L. Pittmann and C. Fleurier, in *Spectral Line Shapes,* edited by K. Burnett (de Gruyter, New York, 1983), Vol. II.

[6]K. H. Finken and U. Ackermann, Phys. Lett. **85A**, 279 (1981).

[7]K. H. Finken and U. Ackermann, J. Phys. D **15**, 615 (1982).

[8]K. H. Finken and U. Ackermann, J. Phys. D **16**, 773 (1983).

[9]H. R. Griem and K. Y. Shen, Phys. Rev. **122**, 1490 (1961).

[10]H. R. Griem, *Plasma Spectroscopy* (McGraw-Hill, New York, 1964).

[11]P. C. Kepple, Phys. Rev. A **6**, 1 (1972).

[12]R. L. Greene, Phys. Rev. A **14**, 1447 (1976).

[13]H. Soltwisch and H. J. Kusch, Z. Naturforsch. **34a**, 300 (1976).

[14]J. E. Bernard, F. L. Curzon, and A. J. Barnard, in *Spectral Line Shapes,* edited by B. Wende (de Gruyter, New York, 1981).

[15]G. V. Sholin, Opt. Spectrosc. **26**, 275 (1969).

[16]A. V. Demura and G. V. Sholin, J. Quant. Spectrosc. Radiat. Transfer **15**, 881 (1975).

[17]H. F. Berg, A. W. Ali, R. Lincke, and H. R. Griem, Phys. Rev. **125**, 199 (1962).

[18]A. Eberhagen and R. Wunderlich, Z. Phys. **232**, 1 (1970).

[19]P. Bogen, Z. Naturforsch. **25a**, 1151 (1970).

[20]J. E. Jenkins and D. D. Burgess, J. Phys. B **4**, 1353 (1971).

[21]D. Einfeldt and G. Sauerbrey, Z. Naturforsch. **31a**, 310 (1976).

[22]T. L. Pittman, P. Voigt, and D. E. Kelleher, Phys. Rev. Lett. **45**, 723 (1980).

[23]M. Baranger, Phys. Rev. **112**, 855 (1958).

[24]M. J. Seaton, *Advances in Atomic and Molecular Physics,* edited by D. R. Bates (Academic, New York, 1975), Vol. 11.

[25]H. A. Bethe, Ann. Phys. (Leipzig) **5**, 3251 (1930); H. van Regenmorter, Astrophys. J. **136**, 906 (1962); H. R. Griem, Phys. Rev. **165**, 258 (1968).

[26]H. R. Griem, Phys. Rev. **165**, 258 (1968).

[27]D. R. Bates and A. Damgaard, Philos. Trans. R. Soc. London, Ser. A **242**, 101 (1949).

[28]G. A. Kobzev, Opt. Spectrosc. **30**, 106 (1971).

[29]M. S. Dimitrijević and N. Konjević, J. Quant. Spectrosc. Radiat. Transfer **24**, 451 (1980).

[30]*Numerical Tables For Angular Correlation Computations in α-, β-, and γ-Spectroscopy: 3j-, 6j-, 9j-Symbols, F- and Γ-Coefficients,* No. I/3-3 of Landolt-Börnstein, edited by H. Schopper (Springer, Berlin, 1968).

[31]S. Sahal-Bréchot and E. R. Serge, Astron. Astrophys. **13**, 1961 (1971).

[32]P. Bogen, Z. Naturforsch. **27a**, 210 (1971).

[33]M. A. El-Farra and T. P. Hughes, J. Quant. Spectrosc. Radiat. Transfer **30**, 335 (1983).

[34]K. Bockasten, Ark. Fys. **10**, 567 (1956).

[35]R. L. Kelly and L. J. Palumbo, U.S. Naval Research Laboratory, Report No. 7599 (1973).

[36]W. L. Wiese, M. W. Smith, and B. M. Glennon, *Atomic Transition Probabilities,* Natl. Bur. Stand. Ref. Data Ser., Natl. Bur. Stand. (U.S.) Circ. No. 4 (U.S. GPO, Washington, D.C., 1966).

[37]C. Jaques, E. J. Kuystantas, R. Drouin, and H. G. Berry, Can. J. Phys. **58**, 1093 (1980).